# A two-step strategy for designing optimal-based active control of human-induced vibrations

Emiliano Pereira[1], Emma J. Hudson[2], Cristina Alén[1], Iván M. Díaz[3] and Paul Reynolds[2,4]

**Abstract**

Civil structures such as floor systems with open-plan layouts or lightweight footbridges can be susceptible to excessive levels of vibrations caused by human activities. Active vibration control (AVC) via inertial-mass actuators has been shown to be a viable technique to mitigate vibrations, allowing structures to satisfy vibration serviceability limits. The application of AVC to complex structures requires the use of several Actuator/Sensor, being necessary the implementation of multiple-input multiple-output (MIMO) strategy. The present work proposes a two-step strategy for designing MIMO optimal-based AVC suitable for structures with a large number of vibration modes and with a large number of test points.

## I. Introduction

Floor systems with open-plan layout and lightweight footbridges are examples of civil structures in which excessive vibrations caused by human activities can occur. Active vibration control (AVC) using inertial-mass actuators has been shown to be a viable technique to impart damping to these structures, especially when the structures are very lively and are excited by a small number of humans, allowing the construction of slender structures leading to significant material savings [1]. The excessive level of vibration is usually a problem of a relatively wide area not just at a single location, which requires the use of several inertial-mass actuators to achieve the vibration reduction requirements. Recently, this was demonstrated in [2], where multiple SISO (single-input single-output) systems were designed. However, the structural system does not act independently at each control location, which results in the need for a reduction of the control gain (and hence performance) of each SISO system to guarantee stability.

A better control performance with the same number of actuators can be obtained if a multiple-input multiple-output (MIMO) strategy is used [3]. However, the simplifications assumed in the design of an optimal control [3] may not viable if the resulting AVC is going to be implemented in practice. Recently, an approach which considers the actuator dynamics (among other issues) has been presented in [4]. This approach has been successfully implemented in practice on an indoor walkway sited at the recently constructed award winning Forum building at the University of Exeter (Exeter, UK). The algorithm presented in [4] is useful when the number of test points is not too high. However, if the number of possible locations of the actuator positioning is large, this algorithm is not convenient due to its high computational cost.

An optimal set of Actuator/Sensor (A/S) locations can be obtained by using $H_2$ and $H_\infty$ norms strategies (see for example [5]). However, although these strategies are useful to obtain a reduced number of nodes where the actuators and sensors can be placed with a low computational cost, the choice of the number of actuators and sensors and the tuning of the MIMO controller are not obvious.

The present work proposes a two-step strategy for designing optimal-based active vibration control for floor and footbridge structures with a large number of test points. Thus, the proposed design strategy finds an optimal set of A/S locations based on $H_2$ norm placement criterion [5] (i.e., reduces the number of test points) to design a MIMO direct velocity feedback by using the control algorithm proposed in [4]. A simulated example, where a finite element (FE) model of a complex floor structure is used, illustrates the computational cost reduction and shows the viability of the design for different numbers of actuators and sensors.

This paper is organised as follows. Section 2 explains an in-service office floor in the UK. Section 3 describes the control scheme elements. Section 4 explains the design methodology. Section 5 provides an application example using the FE model of the structure explained at Section 2. Section 6 concludes the paper.

## II. Structure Model

Before designing and implementing and AVC, It is convenient to carry out an experimental modal analysis (EMA) to obtain an accurate structure model. However, in many cases it is not possible to perform an EMA firstly. Therefore, this paper proposes to design the optimal MIMO AVC based a FE model of the structure. In addition, this section presents a comparison between the models derived by EMA and FE in order to show that model errors are not significant.

*The authors acknowledge the financial support provided by the Fundación Caja Madrid through the grant "II Convocatoria de Becas de Movilidad para profesores de las universidades públicas de Madrid durante el curso académico 2012/2013" and also the UK Engineering and Physical Sciences Research Council (EPSRC) though grant EP/J004081/2 entitled "Advanced Technologies for Mitigation of Human-Induced Vibration"

[1]Emiliano Pereira and Cristina Alén are with Escuela Politécnica Superior, Universidad de Alcalá, ES 28805, Alcalá de Henares, Madrid, Spain emiliano.pereira@uah.es,cristina.alen@uah.es

[2]Emma J. Hudson and Paul Reynolds are with College of Engineering, Mathematics and Physical Sciences, University of Exeter, EX4 4QF, Exeter, UK E.J.Hudson@exeter.ac.uk,p.reynolds@exeter.ac.uk

[3]Iván M. Díaz is with ETS Ingenieros de Caminos, Universidad Politécnica de Madrid, ES 28040, Madrid, Spain b.d.researcher@ieee.org

[4]Paul Reynolds is with Full Scale Dynamics Limited, 40 Leavygreave Road, S3 7RD, Sheffield, UK p.reynolds@exeter.ac.uk

The structure considered in this paper is a steel-concrete composite office floor sited in London (UK). The general arrangement of beams, as shown in Fig. 1(a), has a degree of irregularity but is loosely based on primary steel beams ($PG500 \times 200 \times 241$) at 13 m spacing and secondary steel beams ($PG500 \times 160 \times 94$) at 3 m spacing. The column spacings also have some irregularity but are loosely based on a $13 \times 9$ m grid. A 130 mm lightweight concrete slab, supported by Holorib decking, acts compositely with the steel beams.

The experimental modal analysis (EMA) was performed on the structure using the test grid shown in Figure 1(b). Honeywell QA750 accelerometers were placed at a total of 65 points, located to try and maximise the number of observed modes. 4No. APS-Dynamics actuators (2No. Model 113 and 2No. Model 400) were used to provide excitation at key points within the structure, denoted by triangles on Fig. 1(b). The resulting measured frequency response functions (FRFs) were curve fitted using ME'Scope [6] to derive the mode shapes and frequencies that are shown in Figs. 2 and 3.

The FE model was created in ANSYS [7] using BEAM188 elements for the primary and secondary steel beams and SHELL63 elements for the orthotropic concrete slab. The modal properties were calculated and compared with the results from EMA. It was found that the frequencies from the FE model were too high so some manual model updating was performed. Here, it was decided that the use of lightweight concrete may require a lower Young's Modulus than the 38MPa assumed. Therefore, this was reduced by 20 % to 30.4MPa [2]. This office has a very open-plan layout with the notable exception of a small office and some meeting rooms. The partition for the office, located between gridpoints D5 and E5 on Fig. 1(a) appeared to be significantly increasing the stiffness locally. Therefore, this was explicitly modelled as a glass plate 4mm thick. The partition was attached to a false ceiling rather than the main structural slab, which would have resulted in a loss of effective stiffness. So numerical updating was performed to choose a suitable value of Young's Modulus to represent this; a value of 5GPa was found to match the experimental data best.

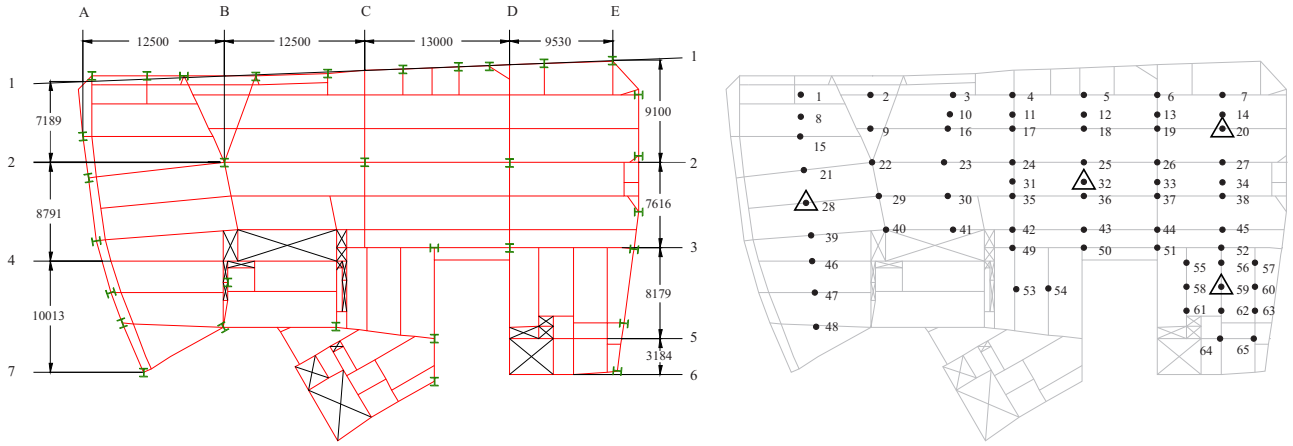


(a) General Arrangement for Structure.

(b) Test Point Locations for Experimental Modal Testing. Triangles denote actuator locations.

Fig. 1. London floor structure.

The updated modal properties for the FE model are compared with those from the EMA in Figs. 2 and 3. It is observed that the mode shapes themselves correlate quite well. However, the frequency values of higher frequency modes are less accurate. Despite this, the accuracy of the model is deemed sufficient to represent the dynamics of the structure well within the frequency range of interest. For the purposes of later simulations, a modal damping ratio had to be assumed for each mode: based on the EMA results, a value of 3 % was used.

## III. Control scheme

This section explains the general scheme shown in Fig. 4 used to define an optimal DVF MIMO control from the proposed optimisation design process. The dynamics included in Fig. 4 are grouped into the following blocks:

1) The flexible structure. The inputs are the force generated by $p$ actuators ($\mathbf{u}_s$) and $r$ perturbations ($\mathbf{w}_s$). The velocity at actuator locations are considered as outputs ($\mathbf{y}_s$).
2) The control gain matrix.
3) The saturation nonlinearity models the actuator force limitation, which is limited by the maximum power amplifier input. This maximum value can be decreased to reduce the risk of stroke saturation but also reducing the actuator performance.
4) The dynamics of the inertial-mass actuators.

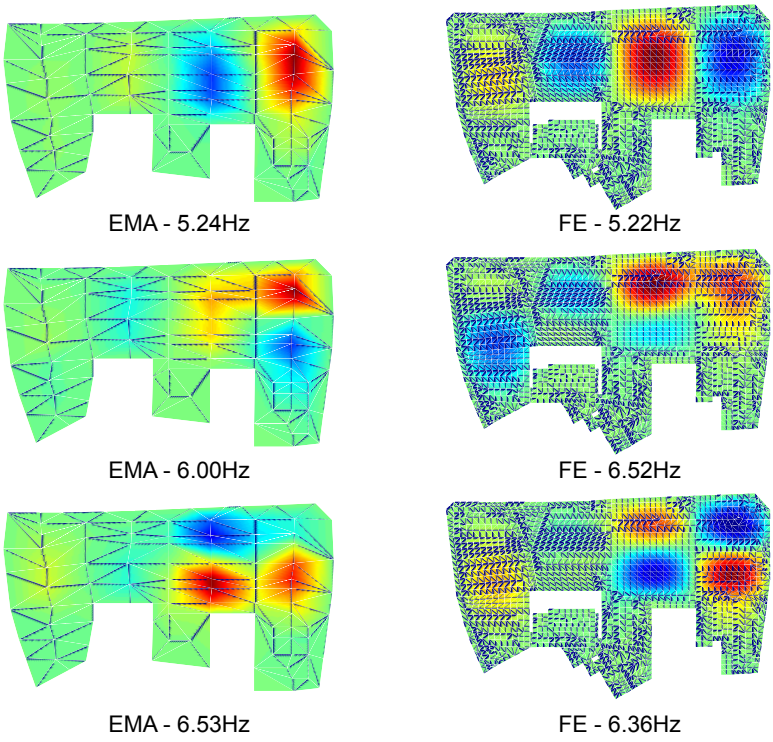


Fig. 2. Comparison between simulated and measured mode shapes (1)

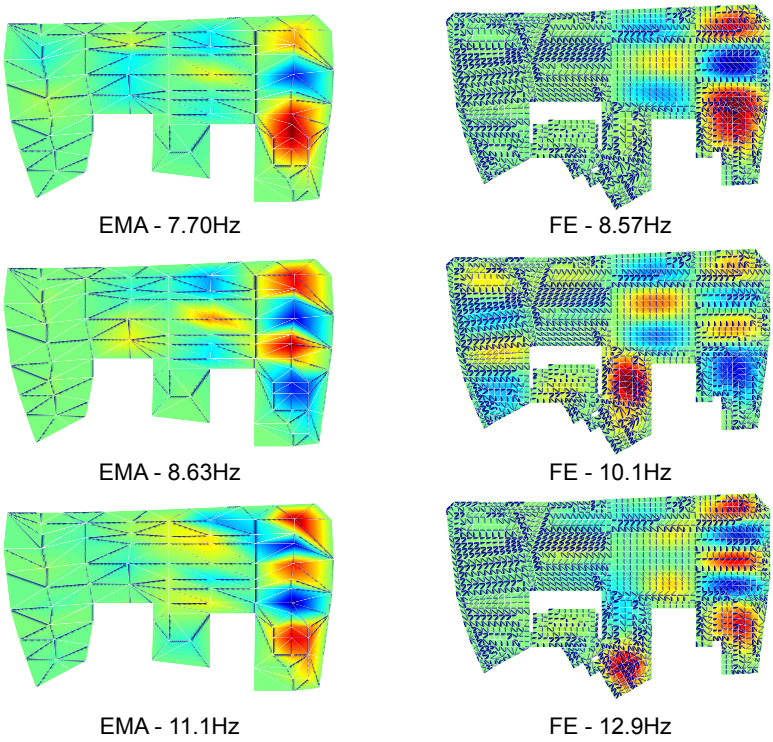


Fig. 3. Comparison between simulated and measured mode shapes (2)

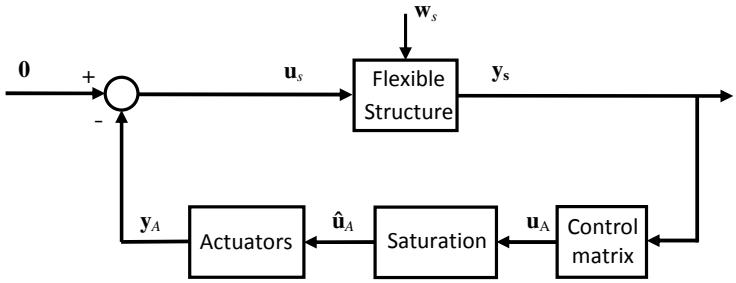


Fig. 4. Control scheme.

*A. Description of the control scheme components*

The standard state-space representation of the model for this flexible structure is represented as follows:

$$\begin{aligned} \dot{\mathbf{x}}_s &= \mathbf{A}_s\mathbf{x}_s + \mathbf{B}_{s_1}\mathbf{u}_s + \mathbf{B}_{s_2}\mathbf{w}_s \\ \mathbf{y}_s &= \mathbf{C}_s\mathbf{x}_s. \end{aligned} \tag{1}$$

If model (1) is defined in modal coordinates, the state-space matrices are as follows [5]:

$$\begin{aligned} \mathbf{A}_s &= \begin{bmatrix} \mathbf{0} & \mathbf{I} \\ -\Omega^2 & -2\mathbf{Z}\Omega \end{bmatrix}, \qquad \mathbf{B}_{s_1} = \begin{bmatrix} \mathbf{0} \\ \Phi_u \end{bmatrix}, \\ \mathbf{B}_{s_2} &= \begin{bmatrix} \mathbf{0} \\ \Phi_w \end{bmatrix}, \qquad \mathbf{C}_s = \begin{bmatrix} \Phi_y & \mathbf{0} \end{bmatrix}, \end{aligned} \tag{2}$$

where $\Omega$ is a $n \times n$ diagonal matrix formed by the natural frequencies ($[\omega_1, \cdots, \omega_n]$), $\mathbf{Z}$ is a $n \times n$ diagonal matrix formed by the damping ratios ($[\zeta_1, \cdots, \zeta_n]$) and $\Phi_u$, $\Phi_y$ and $\Phi_w$ are matrices with dimensions $n \times p$, $q \times n$ and $n \times r$, respectively. Each $k^{th}$ column of $\Phi_u$ and $\Phi_w$ and each row of $\Phi_y$ is formed by the $k^{th}$ vibration mode values at the positions of the actuators ($\Phi_u$), perturbations ($\Phi_w$) and sensors ($\Phi_y$).

The control gain matrix (**K**) in a general form is defined as:

$$K = \begin{bmatrix} K_{11} & K_{12} & \cdots & K_{1q} \\ K_{21} & K_{22} & \cdots & K_{2q} \\ \vdots & \vdots & \ddots & \vdots \\ K_{p1} & K_{p2} & \cdots & K_{pq} \end{bmatrix}, \tag{3}$$

in which $K_{pq}$ is the control gain applied at control input $p$ due to control output $q$.

The outputs of the saturation block, which are the command voltage inputs of the $p$ actuators, are denoted by $\hat{\mathbf{u}}_A$. The actuator considered is an inertial actuator that generates forces through acceleration of an inertial mass to the structure on which it is placed. The actuator consists of an inertial (or moving) mass $m_A$ attached to a current-carrying coil moving in a magnetic field created by an array of permanent magnets. The inertial mass is connected to the frame by a suspension system. The mechanical part is modelled by a spring stiffness $k_A$ and a viscous damping $c_A$. The electrical part is modelled by the resistance $R$, the inductance of the coil $L$ and the voice coil constant $C_E$, which relates coil velocity and the back electromotive force (Fig. 5(a)) [8]. Combining the mechanical and the electrical part, the linear behaviour of the actuator can be closely described as a third-order dynamic model. Thus, the state space model of the $p$ actuators is as follows:

$$\begin{aligned} \dot{\mathbf{x}}_A &= \mathbf{A}_{A_T}\mathbf{x}_A + \mathbf{B}_{A_T}\hat{\mathbf{u}}_A \\ \mathbf{y}_A &= \mathbf{C}_{A_T}\mathbf{x}_A, \end{aligned} \tag{4}$$

being the matrices $\mathbf{A}_{A_T} = diag(\mathbf{A}_A, \cdots, \mathbf{A}_A)$, $\mathbf{B}_{A_T} = diag(\mathbf{B}_A, \cdots, \mathbf{B}_A)$ and $\mathbf{C}_{A_T} = diag(\mathbf{C}_A, \cdots, \mathbf{C}_A)$ block diagonal, where $\mathbf{A}_A$, $\mathbf{B}_A$ and $\mathbf{C}_A$ are defined as follows [9]:

$$\mathbf{A}_A = \begin{bmatrix} 0 & 0 & \varepsilon\omega_A \\ 1 & 0 & \omega_A^2 + 2\zeta_A\omega_A\varepsilon_A \\ 0 & 1 & \varepsilon + 2\zeta_A\omega_A \end{bmatrix}, \ \mathbf{B}_A = \begin{bmatrix} 0 \\ 0 \\ g_A \end{bmatrix}, \ \mathbf{C}_A = \begin{bmatrix} 0 & 0 & 1 \end{bmatrix}, \tag{5}$$

where the actuator is defined by $g_A > 0$, its damping ratio $\zeta_A$ and natural frequency $\omega_A$. The value of $\varepsilon$ models the low-pass properties of the actuator. The actuator in this work is an APS Dynamics Model 400 electrodynamic shaker, which is shown in Fig. 5(b). The identified parameters of (5) are [9]: $\omega_A = 13.2$ rad/s (2.1 Hz), $\zeta_A = 0.5$, $g_A = 12000$ and $\varepsilon_A = 47.1$.

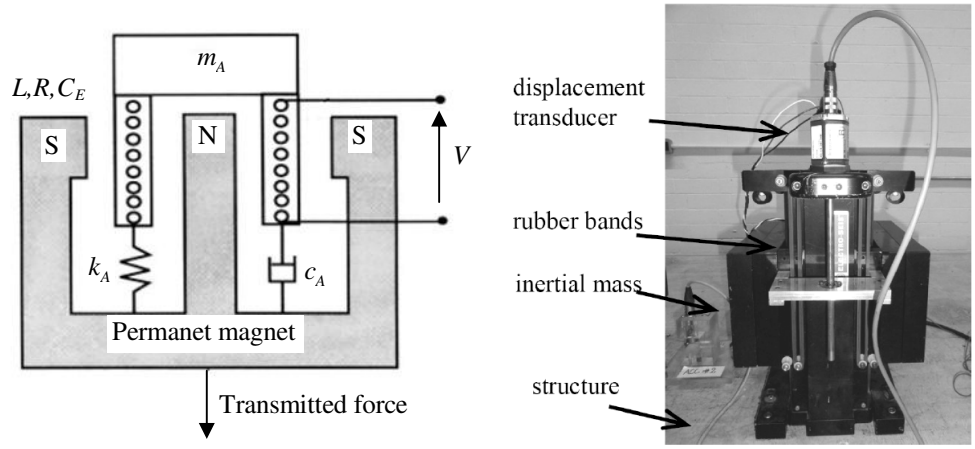


(a) Sketch of typical electrodynamic inertial actuator. (b) APS Dynamics Model 400 Shaker.

Fig. 5. Inertial-mass actuator.

### B. State-space model of the closed-loop system

The state equation of the closed-loop system is obtained from Fig. 4 and (1)-(5), and results in

$$\begin{bmatrix} \dot{\mathbf{x}}_S \\ \dot{\mathbf{x}}_A \end{bmatrix} = \begin{bmatrix} \mathbf{A}_S & -\mathbf{B}_{S_1}\mathbf{C}_{A_T} \\ \mathbf{B}_{A_T}\mathbf{K}\mathbf{C}_S & \mathbf{A}_{A_T} \end{bmatrix} \begin{bmatrix} \mathbf{x}_S \\ \mathbf{x}_A \end{bmatrix} + \begin{bmatrix} \mathbf{B}_{S_2} \\ \mathbf{0} \end{bmatrix} \mathbf{w}_S. \tag{6}$$

The eigenvalues of the $2(n+p)\times 2(n+p)$ state-space matrix are considered into the restrictions defined in the design. These eigenvalues (i.e., the poles of the closed-loop system) are denoted by $-\zeta_{CL_\tau}\omega_{CL_\tau} \pm j\omega_{CL_\tau}\sqrt{1-\zeta_{CL_\tau}^2}$, where $\tau \in [1,\cdots,2(n+p)]$ and $j$ is the imaginary unit.

### C. Human vibration perception

The vibration that can be perceived by a human depends on the direction of incidence to the human body, the frequency content of the vibration (for given amplitude) and the duration of sustained vibration, among other factors. The frequency sensitivity variation for a body position can be taken into account by attenuating or enhancing the system response for frequencies where perception is less or more sensitive, respectively. The degree to which the response is attenuated or enhanced is referred to as frequency weighting. Thus, frequency weighting functions are applied in order to account for the different acceptability of vibrations for different directions and body positions. ISO 2631 [10] and BS 6841 [11] provide details for frequency and direction weighting functions that can be applied which are all based on the basicentric coordinate system shown in Fig. 6. These have been included in current floor design guidelines such as the SCI guidance [12]. According to ISO 2631, for z-axis vibration and standing and seating, the frequency weighting function ($W_k$) is a filter with the frequency response shown in Fig. 7.

Human comfort under vibration is also related to the duration of sustained vibration [13]. Thus, persistent vibrations should be penalised in the control design, giving more importance to transient vibration of long-duration than those of short-duration. This is taken into account by multiplying the system response by an exponential time weighting (i.e., $e^{\alpha t}$), where $\alpha > 0$ adds a constraint in the relative stability of the controlled system. Note that persistent states are penalised more heavily as $\alpha$ is increased.

The human vibration perception is considered in the controller design by weighting the state vector of the structure $\mathbf{x}_S = [x_{s_1},\cdots,x_{s_{2n}}]$ (see (1)) as follows:

$$x_{s_{W_l}} = \left(e^{\alpha t}x_{s_l}(t)\right) * g_{FW}(t),\ l \in [1,\cdots,2n], \tag{7}$$

where (*) denotes the convolution process and $g_{FW}(t)$ is the impulse response function of a system with the frequency response function (FRF) shown in Fig. 7. Note that the weighted vector $\mathbf{x}_{s_W}$ is only used to calculate the PI used to derive the optimal sensor/actuator locations and the gain matrix. In other words, the weighting functions are not included in the closed-loop system of Fig. 4.

## IV. Control design methodology

The design process proposed in this work is based on two steps. Step 1 finds an optimal set of A/S locations based on a $H_2$ norm placement criterion and Step 2 obtains the optimal A/S locations and the control matrix defined in (3).

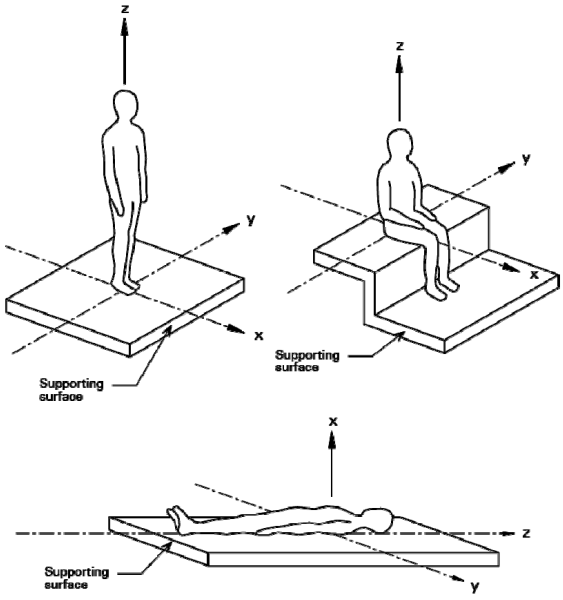


Fig. 6. Directions for vibration according to ISO 2631 [10] and BS 6841 [11] (after [12]).

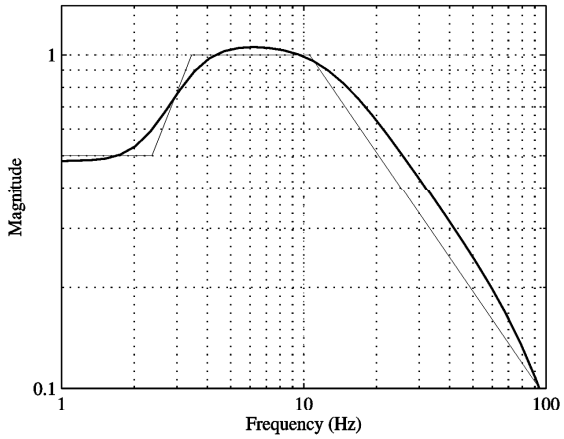


Fig. 7. Frequency weighting function $W_k$ (thicker curve) and its asymptotic definition (thinner curve) [10].

*A. Step 1. $H_2$ norm placement criterion.*

The $H_2$ norm placement criterion considered is based on reference [5]. The objective of this section is to explain how to implement an $H_2$ criterion to find a set of good locations to place the A/S pairs. First of all, let us consider the modal representation of the flexible structure defined in (1)-(2) as follows:

$$\begin{aligned} \dot{\mathbf{x}}_m &= \mathbf{A}_m \mathbf{x}_m + \mathbf{B}_{m_1} \mathbf{u}_s \\ \mathbf{y}_s &= \mathbf{C}_m \mathbf{x}_s. \end{aligned} \tag{8}$$

where the perturbation ($w_s$) is not considered and the matrices $\mathbf{A}_m$, $\mathbf{B}_m$ and $\mathbf{C}_m$ are defined as follows:

$$\begin{aligned} \mathbf{A}_m &= diag\left(\mathbf{A}_{m_1}, \mathbf{A}_{m_2}, \cdots, \mathbf{A}_{m_n}\right), \\ \mathbf{B}_m &= \left[ \begin{array}{cccc} \mathbf{B}_{m_1} & \mathbf{B}_{m_2} & \cdots & \mathbf{B}_{m_n} \end{array} \right]^T, \\ \mathbf{C}_m &= \left[ \begin{array}{cccc} \mathbf{C}_{m_1} & \mathbf{C}_{m_2} & \cdots & \mathbf{C}_{m_n} \end{array} \right], \end{aligned} \tag{9}$$

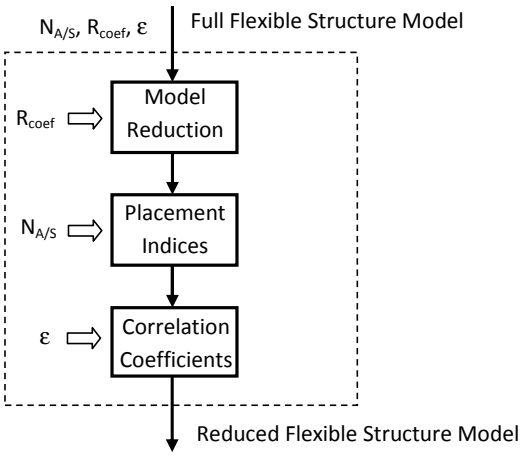


Fig. 8. Step 1.

where $n$ is the number of considered vibration modes and each matrix $B_{m_i}$ and $C_{m_i}$ are defined as follows:

$$\mathbf{A}_{m_k} = \begin{bmatrix} 0 & 1 \\ -\omega_k^2 & -2\xi_k\omega_k \end{bmatrix}, \tag{10}$$

$$\mathbf{B}_{m_k} = \begin{bmatrix} B_{m_{k1}} & B_{m_{k2}} & \cdots & B_{m_{kp}} \end{bmatrix} = \begin{bmatrix} 0 & 0 & \cdots & 0 \\ \phi_{k1} & \phi_{k2} & \cdots & \phi_{kp} \end{bmatrix},$$

$$\mathbf{C}_{m_k} = \begin{bmatrix} C_{m_{1k}} & C_{m_{2k}} & \cdots & C_{m_{qk}} \end{bmatrix}^T = \begin{bmatrix} \phi_{k1} & \phi_{k2} & \cdots & \phi_{kp} \\ 0 & 0 & \cdots & 0 \end{bmatrix}^T,$$

where $\phi_{ki}$ is the mode shape for the $k^{th}$ vibration mode at the $i^{th}$ A/S location.

The $H_2$ norm of the structure is defined as follows:

$$\|G\|_2 \cong \sqrt{\sum_{k=1}^{n} \|G_k\|_2^2}, \tag{11}$$

where $\|G_k\|_2$ is the $H_2$ for a mode. If a set of $q$ sensors and $p$ actuators are defined, the $H_2$ norm for the $i^{th}$ actuator (or sensor) and for the $k^{th}$ mode is

$$H_2 \text{ norm for the } k^{th} \text{ mode and a set of } p \text{ actuators: } \|G_k\|_2 \cong \sqrt{\sum_{i=1}^{p} \|G_{ki}\|_2^2} \tag{12}$$

$$H_2 \text{ norm for the } k^{th} \text{ mode and a set of } q \text{ sensors: } \|G_k\|_2 \cong \sqrt{\sum_{i=1}^{q} \|G_{ki}\|_2^2},$$

where $G_{ki}$ is the $H_2$ norm for the $i^{th}$ actuator (or sensor) and for the $k^{th}$ mode, which is defined as follows:

$$H_2 \text{ norm for the } i^{th} \text{ actuator and for } k^{th} \text{ mode: } \|G_{ki}\|_2 \cong \frac{\|B_{m_{ki}}\|_2^2 \|C_{m_i}\|_2^2}{2\sqrt{\zeta_i\omega_i}} \tag{13}$$

$$H_2 \text{ norm for the } i^{th} \text{ sensor and for } k^{th} \text{ mode: } \|G_{ki}\|_2 \cong \frac{\|B_{m_i}\|_2^2 \|C_{m_{ki}}\|_2^2}{2\sqrt{\zeta_i\omega_i}}.$$

The Step 1, which is shown in Fig. 8, can be divided at: (i) model reduction, (ii) placement indices and (iii) correlation coefficients.

*1) Model reduction:* Then, the number of considered vibration modes are reduced based on the value of the $H_2$ norm of each mode when all the nodes are considered as possible A/S locations. Thus, the model can be defined as follows:

$$\mathbf{A} = \begin{bmatrix} \mathbf{A}_r & \mathbf{0} \\ \mathbf{0} & \mathbf{A}_t \end{bmatrix}, \ \mathbf{B} = \begin{bmatrix} \mathbf{B}_r \\ \mathbf{B}_t \end{bmatrix}, \ \mathbf{C} = \begin{bmatrix} \mathbf{C}_r & \mathbf{C}_t \end{bmatrix}, \tag{14}$$

where $r$ and $t$ means reduced and truncated model, respectively. The error of this model reduction can be defined as follows:

$$e_2 = \|G - G_r\|_2 = \|G_t\|_2 = \sqrt{\sum_{k=n_r+1}^{n} \|G_i\|_2^2}, \tag{15}$$

where $n_r$ is the order of the reduced order model. The model reduction can done by defining a maximum value of $e_2$ or by defining a coefficient $R_{coef}$ with the following restriction:

$$(\|G_k\|_2) / \left( \max_k (\|G_k\|_2) \right) > R_{coef} \tag{16}$$

*2) Placement indices:* The objective is to find the most important nodes for each considered vibration mode. Firstly, a preliminary number of A/S is considered ($N_m$). Secondly, the following $H_2$ placement indices are defined

$$\sigma_{ki} = \frac{\|G_{ki}\|_2}{\|G\|_2}, \tag{17}$$

where $\sigma_{ki}$ is the placement index for the $k^{th}$ vibration mode and $i^{th}$ node. Then, the $N_m$ highest values for each vibration mode are considered. Note that the considered nodes are less or equal to $N_m$ multiplied by the number of vibration modes of the reduced order model.

*3) Correlation coefficients:* This final step analyzes the correlation between the nodes obtained with the placement indices. First of all, the following factor for an $k^{th}$ node is defined:

$$\mathbf{g}_i = \begin{bmatrix} \|G_{1i}\|_2 \\ \|G_{2i}\|_2 \\ \vdots \\ \|G_{ni}\|_2 \end{bmatrix}. \tag{18}$$

Then, the correlation index between the $i^{th}$ and $j^{th}$ is defined as follows:

$$r_{ij} = \frac{\mathbf{g}_i^T \mathbf{g}_j}{\|\mathbf{g}_i\|_2 \left\|\mathbf{g}_j\right\|_2} \tag{19}$$

Finally, the set of possible nodes are obtained by considering the following criterion:

$$I(k) = \begin{cases} 0 & \text{if} \quad r_{ij} > 1-\varepsilon \quad \text{for } \sigma_j \leq \sigma_i \text{ and for } j > 1 \\ 1 & \text{elsewhere} \end{cases} \tag{20}$$

where $\varepsilon$ is a small positive number ($\varepsilon = 0.01 - 0.20$). The nodes with $I(k) = 1$ are taken into account in the optimization algorithm explained in the following section.

*B. Step 2. Optimization algorithm.*

This step is based on the minimisation of a PI related to the dissipation energy of the whole structure due to the AVC action for a given excitation. The PI, which is calculated by using the time and frequency weighted structure states of (7), is defined as follows:

$$J(\mathbf{K}, \Lambda) = \frac{1}{2} \int_0^{t_f} \mathbf{x}_{s_W}^T(\mathbf{K}, \Lambda) \mathbf{Q} \mathbf{x}_{s_W}(\mathbf{K}, \Lambda) dt, \tag{21}$$

where the matrix $\mathbf{Q}$ is a $2n \times 2n$ positive definite matrix, which is taken as [3]

$$\mathbf{Q} = \begin{bmatrix} \omega_1^2 \phi_{1,\max}^2 & \cdots & 0 & 0 & \cdots & 0 \\ \vdots & \ddots & \vdots & \vdots & \ddots & \vdots \\ 0 & \cdots & \omega_n^2 \phi_{n,\max}^2 & 0 & \cdots & 0 \\ 0 & \cdots & 0 & \phi_{1,\max}^2 & \cdots & 0 \\ \vdots & \ddots & \vdots & \vdots & \ddots & \vdots \\ 0 & \cdots & 0 & 0 & \cdots & \phi_{n,\max}^2 \end{bmatrix}, \tag{22}$$

in which $\phi_{k,\max}$ is the maximum value of the $k^{th}$ eigenvector $\phi_k$. Note that the displacement states are weighted by the natural frequencies, thus making the displacement states comparable to the velocity states. The variable $\Lambda$ contains the locations of a set of $p$ actuators and $q$ sensors. Finally, the value of $t_f$ is the simulation time to obtain the PI, which must be large enough to achieve the steady state of $J(\mathbf{K}, \Lambda)$ (i.e., the weighted vector $\mathbf{x}_{s_W} \cong 0$).

The Step 2, which is summarized in Fig. 9, is as follows:

(i) Consider the set of structure nodes obtained at Step 1 and define each possible combination for actuator and sensors. The set of these possible values for $\Lambda$ is denoted by $\Lambda_{PI}$.

(ii) Define the following restrictions to minimize the PI $J = (\mathbf{K}, \Lambda)$: a) $\Lambda \in \Lambda_{PI}$ and b) $0 \leq \alpha \leq \min_k (\zeta_k \omega_k)$, $\forall k \in [1, \cdots, n]$, where the upper limit of $\alpha$ ($\min_k (\zeta_k \omega_k)$) guarantees that the system simulation converges to zero.

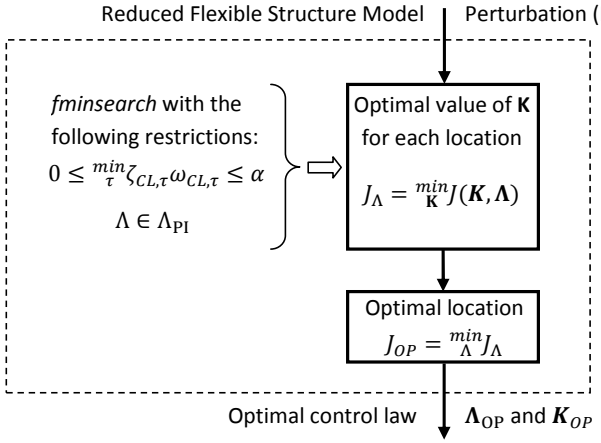


Fig. 9. Step 2.

(iii) Define the system perturbance to assess the controller performance. Note that the design of optimal controllers for unknown disturbances is not trivial since prescribed disturbances are needed within the design process. The solution adopted in this work, similar to that used in [3], is to approximate the influence of zero initial conditions and a spatially distributed, but temporally impulsive, disturbance force by an appropriate initial condition and zero disturbance force. This is achieved by introducing a non-zero initial condition to the velocity states of the structure. Thus, the system perturbance is defined as $\mathbf{x}_s(0) = [x_{s_1} = 0, \cdots, x_{s_n} = 0, x_{s_{n+1}} = \dot{x}_{s_1}(0), \cdots, x_{s_{2n}} = \dot{x}_{s_n}(0)]$, where each value of $\dot{x}_{s_k}(0)$ is obtained as follows:

$$\dot{x}_{s_k}(0) = F_0 \phi_{k,\max}, \tag{23}$$

where $F_0$ represents the impulse loading applied to a particular vibration mode. Note that the impulsive force is applied to the point of maximum amplitude of each vibration mode, creating thus an extreme scenario for the initial disturbance. It is expected that the control system will perform successfully under other loading conditions.

(iv) Find the values of $\Lambda$ and $\mathbf{K}$ that minimize $J(\mathbf{K}, \Lambda)$ of (21). Operationally, it can be divided into the following:

(iv.a) The values of $J$ are obtained for each $\Lambda \in \Lambda_{PI}$ as follows

$$J_\Lambda = \min_{\mathbf{K}} J(\mathbf{K}, \Lambda), \tag{24}$$

where each $J_\Lambda$ is calculated by using the MATLAB function *fminsearch*, which minimises the function defined by the simulation of the control scheme of Fig. 4 with the initial conditions defined by (23), and the restrictions defined at (ii).

(iv.b) The final values of $\mathbf{K}$ and $\Lambda$ are those corresponding to the minimum value of $J_\Lambda$, which is denoted as $J_{OP}$ and is defined as follows:

$$J_{OP} = \min_{\Lambda} J_\Lambda. \tag{25}$$

## V. Application example

The application example consists of designing a MIMO desecentralized control for the structure defined at Section II. Thus, the control matrix defined at (3) is diagonal. Figs. (2) and (3) shows that there are four main bays. Therefore, the number of A/S considered is 4 ($N_{A/S} = 4$). If the FE model described in Section II is used, the structural model has 113 vibration modes and 1653 nodes (test points). This number of modes and nodes makes the Step 2 practically non-implementable. Let us consider the parameters $R_{coef} = 0.75$, $\varepsilon = 0.1$ and $N_{A/S}$ to carry out Step 1, whose results are:

(i) Model reduction reduces the order from $n = 113$ to $n_r = 11$ with an error $e_2 = 0.0071$
(ii) Placement indices reduces the number of test points from 1653 nodes to 44 (see green circles at Fig. 10)
(iii) Correlation coefficients reduces the number of test points from 44 to 13 (see blue circles at Fig. 10)

After Step 1, the possible values for the variables for Step 2 $\Lambda_{PI}$ are obtained as the combination of the 13 test nodes obtained after Step 1. In order to reduce the number of calculations, the combinations are obtained by setting the four A/S as follows:

(i) Actuator A can be placed at $\{(6.18, -2.68), (7.69, -10.63), (7.83, -12.58)\}$.
(i) Actuator B can be placed at $\{(19.29, 3.00), (18.70, -1.99), (17.92, -12.34)\}$.
(i) Actuator C can be placed at $\{(31.93, 4.11), (32.00, 2.00), (32.00, 0.00), (31.00, -3.00), (27.22, -11.46)\}$.

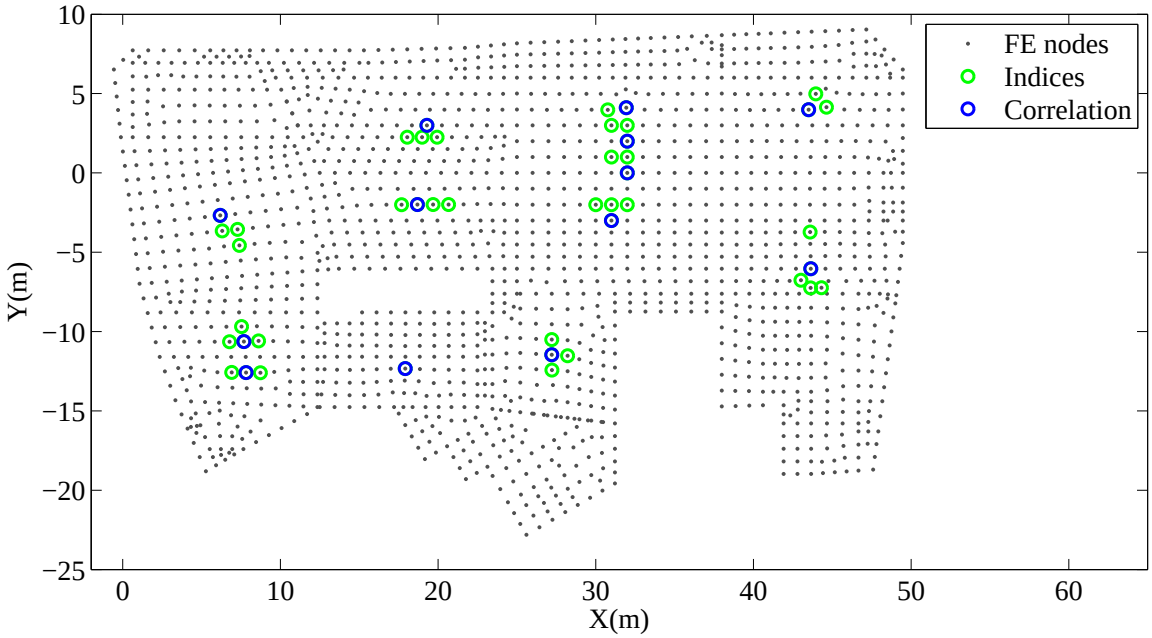


Fig. 10. Test nodes obtained with placement indices (green circles) and correlation coefficients (blue circles).

(i) Actuator D can be placed at $\{(43.50, 3.99), (43.64, -6.04)\}$.

Therefore, Step 2 obtains 90 optimal values of $\mathbf{K}$. These 90 optimal controllers are obtaining by considering $\alpha = 0.25$ and $F_0 = 100$ N. The optimal controller is obtained with $J_{OP} = 0.0018$ and the following location and control matrix:

$$\Lambda_{OP} = \{(6.18, -2.68), (19.29, 3.00), (32.00, 0.00), (43.64, -6.04)\} \tag{26}$$

$$\mathbf{K}_{OP} = \begin{bmatrix} 524 & 0 & 0 & 0 \\ 0 & 919 & 0 & 0 \\ 0 & 0 & 421 & 0 \\ 0 & 0 & 0 & 288 \end{bmatrix},$$

where $\Lambda_{OP}$ are marked at Fig. 11 with red circles. Fig 12 shows the FRF's at optimal nodes ($\Lambda_{OP}$). In order to compare the optimal control, it can be said that the value of functional $J$ is equal to 0.0046. That is, the value of $J_{OP}$ is approximately 36 % of the maximum J. In addition, if the FRF at $\Lambda_{OP}$ are obtained, it can be seen at Fig. 12 the damping reduction with the optimal controller.

## VI. Conclusions

This work presents a novel two-step strategy for designing optimal-based active control for human-induced vibrations. Preliminary results are presented by considering an in-service office floor in the UK with a large number of modes and test points. The results show that an optimal MIMO can be designed systematically and without having a non-implementable computational cost.

The implementation of this technique in practice will be the next work.

## Acknowledgment

The authors acknowledge the financial support provided by the Fundación Caja Madrid through the grant "II Convocatoria de Becas de Movilidad para profesores de las universidades públicas de Madrid durante el curso académico 2012/2013" and also the UK Engineering and Physical Sciences Research Council (EPSRC) though grant EP/J004081/2 entitled "Advanced Technologies for Mitigation of Human-Induced Vibration"

## References

[1] M. J. Hudson and P. Reynolds, "Implementation considerations for active vibration control in the design of floor structures," *Engineering Structures*, vol. 44, pp. 334–358, 2012.

[2] E. J. Hudson and P. Reynolds, "Implications of structural design on the effectiveness of active vibration control of floor structures," *Structural Control and Health Monitoring*, vol. 21, no. 5, pp. 685–704, 2014. [Online]. Available: http://dx.doi.org/10.1002/stc.1595

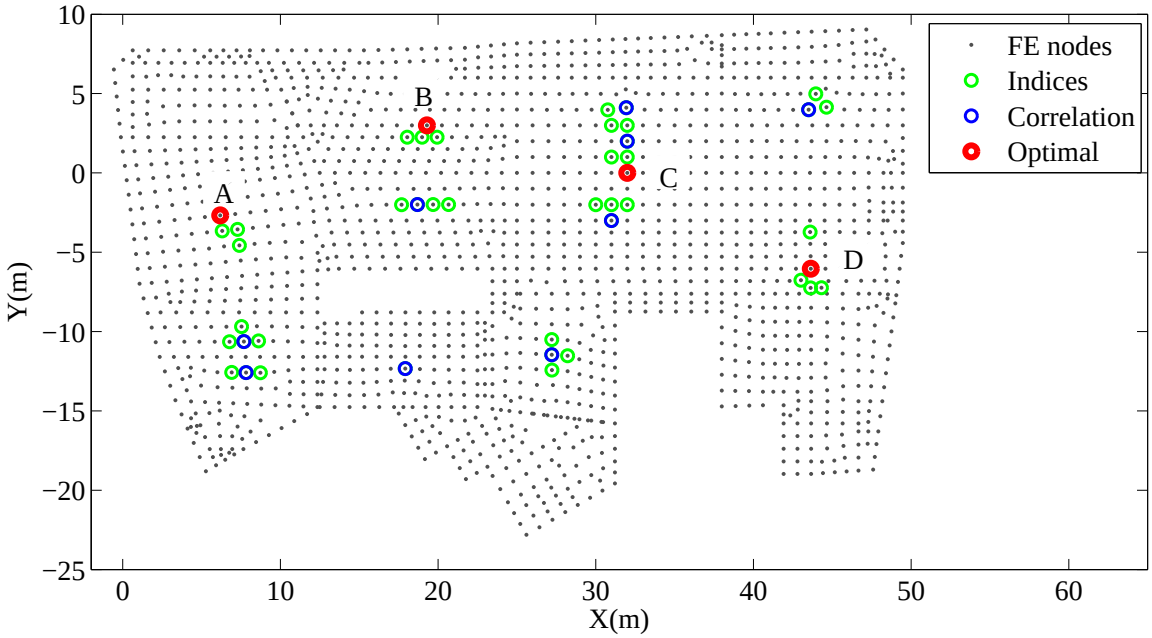


Fig. 11. Test nodes obtained with placement indices (green circles), correlation coefficients (blue circles) and Step 2.


[3] L. M. Hanagan, E. C. Kulasekere, K. S. Walgama, and K. Premaratne, "Optimal placement of actuators and sensors for floor vibration control," *Journal of Structural Engineering*, vol. 126, no. 12, pp. 1380–1387, 2000.

[4] E. Pereira, I. M. Díaz, E. J. Hudson, and P. Reynolds, "Optimal control-based methodology for active vibration control of pedestrian structures," *Engineering Structures (submitted for publication)*.

[5] W. K. Gawronski, *Advanced Structural Dynamics and Active Control of Structures*. Springer-Verlag, 2004.

[6] Vibrant Technology Inc., "ME'ScopeVES 4.0 Tutorial," 2003.

[7] ANSYS, "Release 11.0 Documentation for ANSYS," 2000.

[8] A. Preumont, *Vibration control of active structures: an introduction*. Kluwer Academic Publishers, 2002.

[9] I. M. Díaz and P. Reynolds, "Acceleration feedback control of human-induced floor vibrations," *Engineering Structures*, vol. 32, no. 1, pp. 163–173, 2010.

[10] ISO2631-1, *Mechanical vibration and shock - Evaluation of human exposure to whole-body vibration. Part 1: General requirements*. International Organization for Standardization, 1997.

[11] BS6841, *Guide to measurement and evaluation of human exposure to whole-body mechanical vibration and repeated shock*. British Standards Institute, 1997.

[12] A. L. Smith, S. J. Hicks, and P. J. Devine, *Design of floors for vibration: A new approach ( P354)*. The Steel Construction Institute, 2007.

[13] K. Lenzen, "Vibration of steel joist-concrete slab floors," *Engineering Journal, AISC*, vol. 3, no. 3, pp. 133–136, 1966.

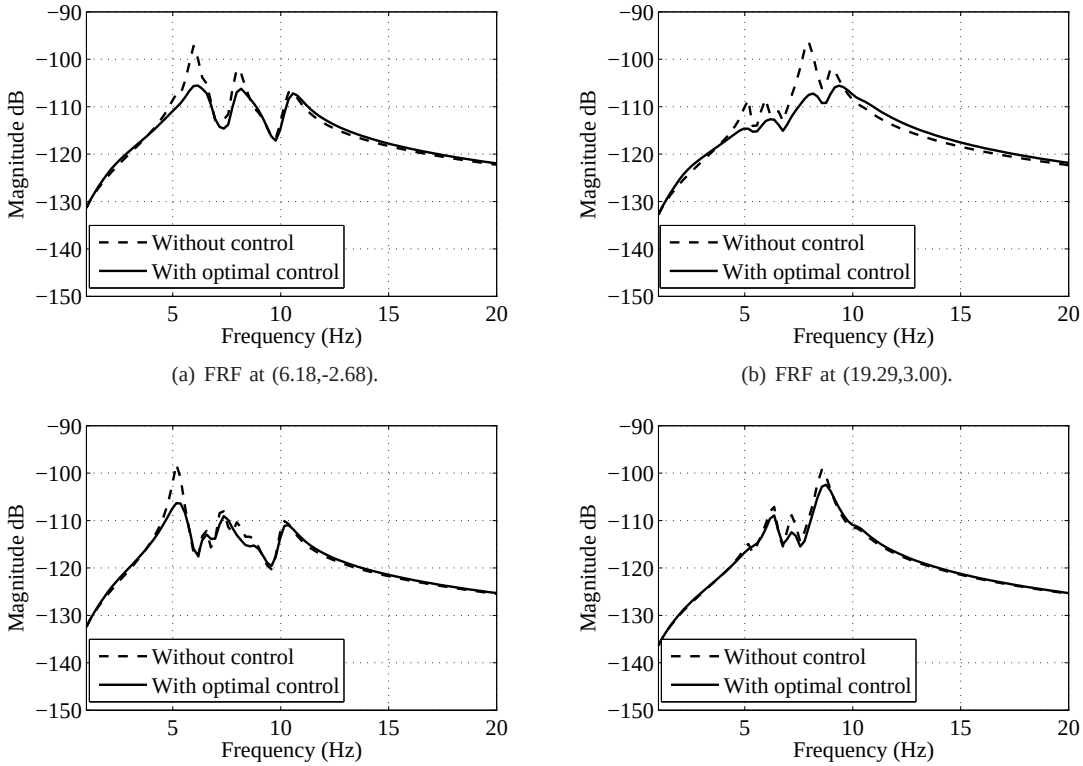


(a) FRF at (6.18,-2.68).

(b) FRF at (19.29,3.00).

(c) FRF at (32.00,0.00).

(d) FRF at (43.64,-6.04).

Fig. 12. FRF's at $\Lambda_{OP}$.